

# Spectroscopic Variability of the Compact Planetary Nebula Hb 12

N.P. Ikonnikova<sup>1\*</sup>, I.A. Shaposhnikov<sup>1,2</sup>, V.F. Esipov<sup>†</sup>, M.A. Burlak<sup>1</sup>,  
V.P. Arkhipova<sup>1</sup>, A.V. Dodin<sup>1</sup>, S.A. Potanin<sup>1,2</sup>, and N.I. Shatsky<sup>1</sup>

<sup>1</sup>*Sternberg Astronomical Institute, Moscow State University (SAI MSU), Moscow, 119234  
Russia*

<sup>2</sup>*Faculty of Physics, Moscow State University, Moscow, 119991 Russia*

We present the results of our new low-resolution spectroscopic observations of the young compact planetary nebula Hb 12 performed in 2011–2020 with SAI MSU telescopes. We have measured the intensities of more than 50 nebular emission lines in the spectral range  $\lambda 3687$ – $9532$ , detected interstellar absorption features, and conducted a search for absorptions belonging to the possible secondary component of the central star. The extinction coefficient has been estimated from the Balmer decrement to be  $c(\text{H}\beta) = 1.15 \pm 0.07$ . The distance has been found by analyzing the interstellar extinction maps to be  $D \approx 2400$  pc. We have traced the history of the spectroscopic observations of Hb 12, beginning with the first spectra taken by Aller (1951) in 1945. We have detected a systematic increase in the relative intensities of the nebular [O III]  $\lambda 4959$  and  $\lambda 5007$  lines and a decrease in the relative intensity of the auroral [O III]  $\lambda 4363$  line, which has led to an increase in the observed flux ratio  $F(\lambda 4959 + \lambda 5007)/F(\lambda 4363)$  by a factor of  $\sim 4$  from 1945 to the present time. The [O III]/[O II] line ratio  $F(\lambda 4363)/F(\lambda 3727 + \lambda 3729)$  remains constant, suggesting that the degree of ionization, on average, for the nebula is invariable. The temperature of the exciting star has been estimated to be  $T \approx 41\,000$  K. We conclude that a decrease in the electron temperature and, possibly, electron density in the [O III] line formation region is mainly responsible for the spectroscopic variability.

*Keywords:* planetary nebulae, spectroscopic variability, Hb 12, gaseous-envelope parameters, evolution.

---

\*ikonnikova@gmail.com

# INTRODUCTION

Planetary nebulae (PNe) are a product of the late evolution of low- and moderate-mass ( $M \sim 0.8 - 8.0M_{\odot}$ ) stars. The lifetime of such stars in the post-asymptotic giant branch (post-AGB) stage of evolution depends on the stellar mass and the mass loss rate on the asymptotic giant branch (AGB) and can range from 100 to several thousand years. The interest in studying the observational manifestations of the evolution of post-AGB stars and young planetary nebulae has increased significantly in recent years owing to the construction of new evolutionary models by Miller Bertolami (2016), whose time scales are several-fold shorter than those in previous models (Vassiliadis and Wood 1994; Blöcker 1995).

Several objects the change of whose emission-line spectra can be caused by a rise in the temperature of the exciting star, consistent with the idea of rapid evolution in the post-AGB stage, have already been discovered. For example, the compact low-excitation PN Hen 2-260 has shown a change of its spectrum in the last 30 years: in the mid-1980s no nebular emission lines were detected in its spectrum (Acker et al. 1991), in 2001 the [O III]  $\lambda 5007$  line flux was 5 % of the  $H\beta$  flux (Escudero et al. 2004), while in 2012 it was already about 7 % (Hajduk et al. 2014). The authors of the latter paper believe that the strengthening of nebular lines is related to the increase in the degree of ionization in the nebula because of a rise in the temperature of the exciting star.

There exist PNe whose spectroscopic variability is associated not with the evolution of the central star, but with the change in gaseous-envelope parameters due to a separate episode of enhanced mass loss by the nonstationary PN nucleus. IC 4997, for which the spectroscopic observations have been carried out for more than half a century (Kostyakova and Arkhipova 2009; Arkhipova et al. 2020), may serve as a striking example of such PNe. What provoked the stellar-wind strengthening, whether this was a single event, and whether it will be repeated again such form or another remains an open question.

Kondratyeva (2005) detected significant changes in two PNe, M 1-6 and M 1-11, based on 30–35 years of observations. In the opinion of this author, a significant strengthening of the [O III] and He I lines and a weakening of the [S II] line (in M 1-6) suggest a change of the physical conditions in the nebulae. It is reasonable to assume that all of the observed effects were caused by an increase in  $T_{\text{eff}}$ , but the available estimates of this stellar parameter do not confirm this hypothesis. For M 1-11 sudden increases in  $N_e(\text{S II})$ ,  $T_e(\text{O III})$ , and  $T_e(\text{N II})$  were recorded in 1996. The author assumes that these changes are associated with some dynamic events in the nebula.

The goal of this paper was to check the possible spectroscopic variability of the young compact PN Hb 12.

The PN Hb 12 (also known as PNG 111.8-02.8, VV 286, the Matryoshka nebula) was discovered by Edwin Hubble 100 years ago (Hubble 1921). This object is characterized by a complex bipolar structure and compact sizes: the angular diameter of the optically brightest part of the nebula is  $2''-3''$ , the region of weak  $H\alpha$  emission extends approximately to  $13''$  (Miranda and Solf 1989). Kwok and Hsia (2007) studied the nebular structure in the [N II] line based on Hubble Space Telescope observations. Subsequently, Vaytet et al. (2009) created a morpho-kinematical model of Hb 12 based on imaging and high-resolution long-slit spectroscopy. The authors for the first time revealed the presence of end caps (or knots) in a deep [N II]  $\lambda 6584$  image of Hb 12 and measured their radial velocities,  $\sim 120$  km/s. Clark et al. (2014) presented near-infrared (IR) spectroscopic observations of Hb 12 using the Near-infrared Integral Field Spectrograph (NIFS) on Gemini-North. Combining NIFS with the adaptive optics system Altair, the authors studied in detail the inner structure of the nebula.

The PN Hb 12 stands out for its low metallicity (Faúndez-Abans and Maciel 1986; Perinotto 1991; Hyung and Aller 1996; Kwitter et al. 2003) and belongs to the Galactic thin disk. Given its chemical composition, location in the Galaxy, and kinematical characteristics, Quireza et al. (2007) classified Hb 12 as a type IIa PN according to Peimbert (1978).

The central star may be a close binary system with an orbital period of 3.4 h (Hsia et al. 2006); the effective temperature of the PN nucleus is estimated to be 42 000 K (Preite-Martinez and Pottasch

1983).

The PN Hb 12 has a significant far-IR excess and was identified with the IR source IRAS 23239+5754. Zhang and Kwok (1991) constructed the spectral energy distribution of the object in a wide wavelength range, from 0.1 to 100  $\mu\text{m}$ , and ascribed the IR excess to the radiation of dust with  $T_{\text{dust}} = 203$  K. Subsequently, Jiang et al. (2013) analyzed the spectrum of Hb 12 based on observations from the Spitzer satellite with the IRC spectrograph and detected a set of silicate emission features with a predominance of enstatite ( $\text{MgSiO}_3$ ) in the spectral range 9.9-37.2  $\mu\text{m}$ .

The basic known data on the object are given in Table 1.

The history of the spectroscopic study of Hb 12 spans 75 years since the time when L. Aller took the first spectrograms of the nebula at the Lick Observatory on July 2, 1945. The measurements of the relative intensities of 16 emission lines in the spectral range from 3727 to 5007  $\text{\AA}$  are presented in Aller (1951).

Hb 12, along with other PNs, fell into various spectrophotometric surveys: the photoelectric photometry of 34 PNe (O'Dell 1963), the photographic and photoelectric spectrophotometry of the blue part of the optical spectral range for 21 nebulae (Kaler et al. 1976), the photoelectric measurements of emission line intensities for 36 nebulae (Barker 1978), and the photoelectric spectrophotometry of 8 compact nebulae (Ahern 1978). Note also the paper of Kwitter et al. (2003), where the spectra of 21 objects, including the nebula Hb 12, were analyzed to study the relative abundances of various elements in PNe.

The most comprehensive and detailed study of a high-resolution spectrum for Hb 12 in the range 366-1005 nm was carried out by Hyung and Aller (1996). In particular, these authors determined the physical parameters and chemical composition of the nebula and constructed its spatial model. Based on high-resolution spectra, Miranda and Solf (1989) studied the kinematical and geometrical structure of Hb 12.

Luhman and Rieke (1996) studied in detail the near-IR spectrum of Hb 12. Subsequently, Hb 12 was among the 72 PNe for which spectroscopic observations were performed in the wavelength range 2.5-5.0  $\mu\text{m}$  with the Infrared Camera (IRC) onboard the AKARI satellite (Ohsawa et al. 2016).

The important question about the possible PN nucleus binarity remains open. The bipolar structure of the emitting PN envelope implies the presence of a binary star system as a consequence of the influence of its gravitational field on the gas expansion. However, no other reliable confirmations of the existence of a companion, except for the paper by Hsia et al. (2006), where the possible binarity of the central star of Hb 12 was studied based on photometric and spectroscopic observations, have been obtained so far for Hb 12. The authors of the mentioned paper deem the presence of a secondary component proven and even provide an estimate of its mass and orbital parameters, but the results of this study came under criticism in De Marco et al. (2008).

This paper is devoted to the analysis of long-term spectroscopic observations of Hb 12 aiming to study the possible variability of the object.

Table 1: Basic data on the PN Hb 12

Parameter	Value	Source
Equatorial coordinates (J2000) (J2000)	$\alpha = 23^{\text{h}}26^{\text{m}}14.8^{\text{s}}$ , $\delta = +58^{\circ}10'54.5''$	SIMBAD
Galactic coordinates (J2000) (J2000)	$l = 111.^{\circ}88$ , $b = -2.^{\circ}85$	SIMBAD
Radial velocity	$\sim -5.0$ km/s	SIMBAD
Excitation class	4	Hyung and Aller (1996)
Characteristics of the central star	$B = 14.^{\text{m}}5$ , $V = 13.^{\text{m}}8$ , $\log g = 5.5$ , $R = 3.0R_{\odot}$ , $L = 1200L_{\odot}$	Hyung and Aller (1996)
Expansion velocity of the central region	$\sim 16$ km/s	Miranda and Solf (1989)
Kinematic age	300 years	Miranda and Solf (1989)
Mass of the HII region	$0.05 M_{\odot}$	Miranda and Solf (1989)

Table 2: Log of observations

Designation	Date	JD	Number of frames	Exposure time, s	Standard
CAS, Zeiss + ST-402					
11	Aug. 26, 2011	2455800	21	60, 300, 900	BS 8606
15	Aug. 13, 2015	2457248	21	60, 600, 900, 1200	1 Cas
16	Oct. 5, 2016	2457667	19	30, 60, 600, 1200	12 Cas
17	Aug. 20, 2017	2457986	19	60, 300, 1200, 1800	12 Cas
18	Oct. 8, 2018	2458400	10	60, 300, 1800	12 Cas
19	July 26, 2019	2458690	24	30, 60, 120, 600, 1800	BS 8606, HD 211073
CAS, Canon + FLI					
19a	Aug. 7, 2019	2450702	6	30, 300, 600, 1800	BS 8606, $\tau$ Cas
19b	Oct. 1, 2019	2458758	5	30, 60, 1800	4 Lac
CMO					
19c	Nov. 7, 2019	2458795	26	5, 20, 60	BS 8606
20	Jan. 20, 2020	2458869	39	1, 3, 5, 30, 60, 300	Hilt600

## OBSERVATIONS AND DATA REDUCTION

The spectroscopic observations of the PN Hb 12 in 2011–2019 were carried out with the 1.25-m telescope at the Crimean Astronomical Station (CAS) of the SAI MSU using a spectrograph with a 600 lines/mm diffraction grating and a long slit of width 4'' in the range 4000–9000 Å. The full recorded spectrum consists of several overlapping ranges. The observations were carried out with several exposure times. The minimum exposure time was chosen so that the strongest lines (H $\alpha$  and [O III]  $\lambda$ 5007) were not overexposed. On the observing night we imaged a star, a secondary spectrophotometric standard, at a close airmass together with the object for the subsequent flux calibration of its spectra. An ST-402 765×510 pixel CCD (pixel size 9×9  $\mu$ m) was used as the detector. The spectral resolution (FWHM) was 7.4 Å.

In 2019 the instrumentation was upgraded, as a result of which a Canon lens and a FLI PL-4022 2048×2048 pixel CCD were installed on the spectrograph instead of the Zeiss lens and the ST-402 CCD. As a result, the vignetting virtually disappeared, the simultaneously recorded spectral range expanded, the image quality improved, and the signal-to-noise ratio increased, especially in the blue part of the spectrum.

The spectra were reduced with the standard CCDOPS software and the SPE software created at the Crimean Astrophysical Observatory (Sergeev and Heisberger 1993). We performed absolute flux calibration based on the spectra of a standard star from the spectrophotometric catalogue by Glushneva et al. (1998) using data from the atlas of standard stellar spectra by Pickles (1985).

In addition, in November 2019 and January 2020 we took spectra in the range 3500–7500 Å with the 2.5-m telescope at the Caucasus Mountain Observatory (CMO) of the SAI MSU using a new low-resolution double-beam spectrograph (TDS) equipped with volume phase holographic gratings. Andor Newton 940P cameras with a E2V CCD42-10 512×2048 pixel arrays are used as the detectors. A detailed description of the instrument is given in Potanin et al. (2020). The observations were carried out with a long slit of width 1.''0. The data reduction included the bias subtraction, flat fielding, and dark current subtraction. Cosmic-ray hits were removed from the two-dimensional spectrogram. To correct for the detector spectral efficiency, atmospheric and optics transmission, we observed the spectra of standards for which the absolute spectral energy distribution was retrieved from the library<sup>1</sup>. The entire reduction was performed using self-developed Python scripts.

A log of spectroscopic observations is presented in Table 2.

The emission line fluxes were determined by two methods: spectral profile integration and Gaussian fitting (this technique was applied mainly to blends and strong lines). Initially, these quantities were

<sup>1</sup><https://www.eso.org/sci/observing/tools/standards/spectra/stanlis.html>

determined in absolute energy units; subsequently, for convenience, they were converted to the relative scale of  $F(H\beta)=100$ . If at one date of observations a specific line was reliably measured simultaneously on several frames, then the values obtained were averaged and the error was calculated as the rms deviation from the mean in a given sample. The accuracy of measuring the intensity of an individual line was about 10 % for the spectrograms taken in Crimea before the lens replacement, about 7-8 % after the lens replacement, and 5-6 % for the CMO spectra.

## DESCRIPTION OF THE SPECTRUM

For each set of CAS spectra we identified  $\sim 50$  emission lines and measured their fluxes. The nebular [O III]  $\lambda 4959$  and  $\lambda 5007$ , Balmer hydrogen lines, forbidden [O I], [O II], [O III], [N II], [S II], [Ar III] lines, and He I recombination lines are the most intense ones. In addition, there are permitted O I, O II, N II, and N III lines in the spectrum. The Paschen and forbidden [S III] lines (measured in the 2011, 2017, and 2018 spectra) are strong in the near infrared. In some spectra we managed to identify and measure weak [Si II], [Cl III], [Fe III], and some other ion lines, but the measurement errors of their intensities are fairly large. An example of the spectrum taken in Crimea is presented in Fig. 1.

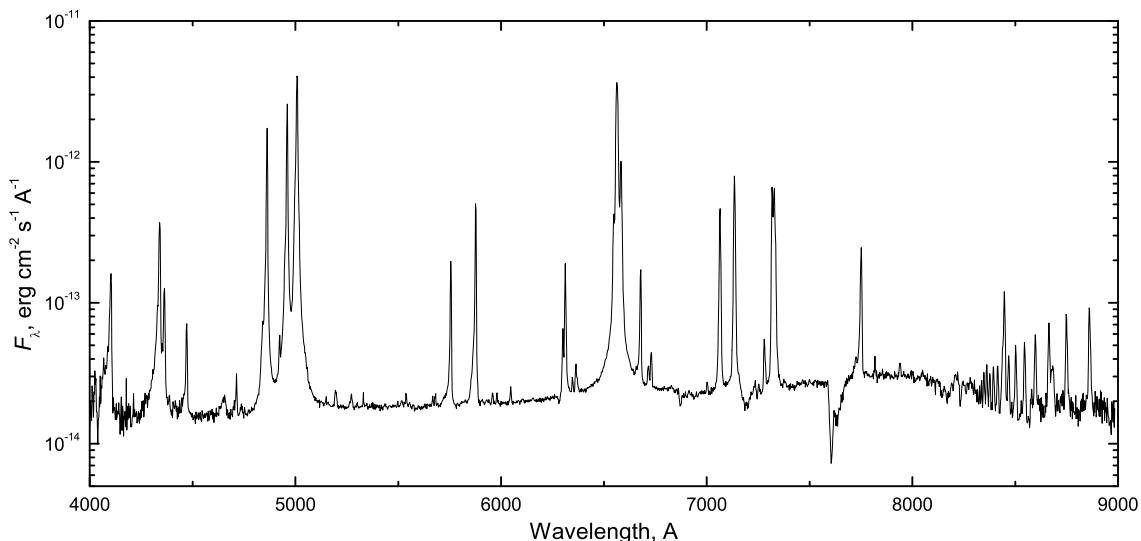


Figure 1: The CAS SAI spectrum of Hb 12 taken on August 13, 2015.

Compared to the technical capabilities of the CAS, the instrumentation installed on the 2.5-m CMO telescope allows spectra with a better resolution and a higher signal-to-noise ratio to be obtained in a shorter exposure time. The blue and red ranges are recorded simultaneously; the blue range was extended to short wavelengths. Thus, new opportunities for a spectral analysis open up. Figures 2 and 3 present fragments of the CMO spectrum in the wavelength ranges 3600–5200 Å and 5500–7500 Å, respectively.

In the CMO spectra in the blue part ( $\lambda < 4000$  Å) the Balmer hydrogen lines and He I lines dominate and there are permitted OI lines and forbidden [O II], [S III], and [Ne III] lines. Based on these data, we also managed to measure the intensity of the weak He II  $\lambda 4686$  line. At a wavelength near  $\lambda 4640$  we see a group of N II, N III, and O II lines. They probably belong to the central star and allow it to be attributed to the PN cores with weak emissions in the spectrum (the so-called *wels*, weak emission-lines star) segregated by Tyllenda et al. (1993) into a separate subclass of central stars.

The CMO spectrograms allowed us to measure the height of the Balmer jump and to determine the electron temperature of the nebula (see the corresponding section).



the nebula Hb 12 is binary remains open.

The spectroscopic data for Hb 12 obtained during the 2011–2020 observations are presented in the Appendix. The first two columns give the wavelength (to within 1 Å) and the corresponding species. The F(year) columns give the observed (without any correction for interstellar extinction) relative line intensities, where by "year" we mean a separate data set (see the "Designation" column in Table 2).

## CHANGE OF THE SPECTRUM WITH TIME

To keep track of how the spectrum of Hb 12 changed with time, we used the data from Aller (1951), O'Dell (1963), Kaler et al. (1976), Ahern (1978), Barker (1978), Hyung and Aller (1996), Kwitter et al. (2003), and Hajduk et al. (2015) and compared them with our observations performed at CAS in 2011–2019 and at CMO in 2019–2020.

Hb 12 is a compact PN: the size of its brightest central region does not exceed 4". The size of the slit or circular aperture used in the observations is not always specified in the literature. For those cases where this information is available, obviously, the nebula entirely fell into the spectrograph slit. This is also true for our observations performed in 2011–2019 at CAS. In 2019–2020 the spectra were taken at CMO with a narrower slit. However, our quasisimultaneous 2019 observations at CAS and CMO showed that both the absolute  $H\beta$  flux and the relative emission line intensities are in good agreement, within the measurement error limits. This gives us the right to include the CMO data for 2019–2020 in our comparative analysis as well.

Table 3 gives a compilation of the relative intensities of some emission lines from Barker (1978), Hyung and Aller (1996), and Kwitter et al. (2003), along with our new data. The CAS column provides the averaged data obtained at the ZTE telescope in 2011–2019. The CMO column presents the relative line intensities measured in the 2019–2020 spectra. Apart from these studies, we took into account the data from all of the papers listed at the beginning of the section when analyzing the changes in the spectrum of Hb 12.

Let us consider how the absolute  $H\beta$  flux behaves with time (Fig. 4). On the whole, it can be said that the  $H\beta$  flux did not change in the time of observations. However, some dip that, if the measurement of Barker (1978) is taken into account, could reach an order of magnitude is noticeable on the graph. It exhibits no apparent correlation with the changes in the relative intensities of other emission lines and, therefore, its nature remains unclear.

By analyzing the data presented in Table 3, we can conclude that the relative intensity of the He I  $\lambda 5876$ ,  $\lambda 6678$ , and  $\lambda 7065$  lines has not changed significantly over the period under consideration (from the first half of the 1970s to the present time). The data for He I  $\lambda 4471$  are available for a longer time interval, beginning from 1945 (Aller 1951), and they suggest a possible decrease in the relative intensity of this line (Fig. 5). The He II  $\lambda 4686$  emission line in the spectrum of Hb 12 is weak, and it was measured only by Barker (1978) and Hyung and Aller (1996). In the CMO spectra we managed to measure this line quite reliably. As regards the behavior of He II  $\lambda 4686$ , no changes outside the error limits have been revealed so far in a short time interval. It is expected that the He II line will strengthen as the central star evolves.

Consider the behavior of forbidden lines. The relative intensities of the [Ar III]  $\lambda 7135$  and  $\lambda 7751$  lines and the forbidden  $S^{+2}$   $\lambda 6312$  line apparently remain constant so far. It is worth treating the possible time dependence of the intensity for the forbidden [O I]  $\lambda 6300$  and  $\lambda 6363$  lines with caution because of the strong scatter in the data obtained by different authors.

In the time of spectroscopic observations the relative intensity of the [Ne III]  $\lambda 3869$  line (Fig. 6) slightly decreased, but these estimates also have a significant scatter.

The time dependence of the relative intensities of the [O II]  $\lambda 3727$  and  $\lambda 3729$  doublet lines is plotted in Fig. 7. In view of the closeness of these lines in most of the papers where the spectrum of Hb 12 was studied, including our paper, the sum of these lines was measured. Despite the significant scatter of data points, a falling trend can be distinguished on the graph. The behavior of the IR [O II]  $\lambda 7320$  and  $\lambda 7330$  doublet also shows a similar picture (see Table 3).

Table 3: Observed relative intensities of emission lines in the spectrum of Hb 12 on the scale of  $F(\text{H}\beta) = 100$  and logarithm of the observed  $\text{H}\beta$  flux in  $\text{erg s}^{-1} \text{cm}^{-2}$

Source		Barker 1978	Hyung and Aller 1996	Kwitter et al. 2003	CAS	CMO
year		1972	1990	1997	2011-2020	2019-2020
$\lambda$ , Å	Species					
3727+29	[O II]	10.7	4.75	7.2	-	5.93
3869	[Ne III]	38	38.28	34	-	33.9
4101	H I	18.5	18.79	18	14.4	15.4
4340	H I	33.9	35	33.4	34.3	35.4
4363	[O III]	15.7	15	11.5	9.8	10.1
4471	He I	4.58	4.79	4.2	3.6	4.5
4686	He II	0.3	0.07	-	-	0.14
4861	H I	100	100	100	100	100
4959	[O III]	144	168.27	160	185	188
5007	[O III]	449	566.24	515	577	601
5192	[Ar III]	-	0.31	-	0.41	0.23
5517	[Cl III]	-	0.08	0.1:	-	0.08
5537)	[Cl III]	-	0.21	0.2:	0.31	0.30
5755	[N II]	12.2	13.12	12.3	10.4	12.0
5876	He I	29.6	34.28	30.7	28.9	31.6
6300	[O I]	15	2.1	2.8	2.9	2.7
6312	[S III]	-	13.4	11	8.6	9.0
6363	[O I]	2.41	0.9	1.2	0.98	0.88
6548	[N II]	-	17.22	23.7	-	20.1
6563	H I	752	1013.9	684	663	861
6583	[N II]	68.1	60.81	63.9	74	61
6678	He I	9.59	12.11	9.3	9.9	11
6717	[S II]	0.96	0.3:	0.9	0.62	0.44
6731	[S II]	1.57	1.0:	1.6	1.28	0.88
7065	He I	-	42.85	36.4	34	38.7
7135	[Ar III]	-	72.11	62.8	61	62.6
7320+30	[O II]	124	135.25	118	103	113.7
7751	[Ar III]	-	18.88	18	17.4	-
9069	[S III]	-	124.17	117	105	-
$\lg(F(\text{H}\beta))$	H I	-12.00±0.01	-	-10.96±0.04	-10.95±0.02	-10.91±0.03

The behavior of forbidden [O III] lines, namely the nebular  $\lambda 5007$  and  $\lambda 4959$  lines and the auroral  $\lambda 4363$  line, deserves special attention. These lines are among the strongest and reliably measured ones, and they are more sensitive to a change in the parameters of the gaseous envelope and the central star than others. Probably, there is, first, an increase in the relative intensities of the  $\lambda 4959$  and  $\lambda 5007$  lines and, second, a decrease in the ratio  $F(\lambda 4363)/F(\text{H}\beta)$  over the period under consideration. Figure 8 plots the dependence of the relative observed [O III] line fluxes on the epoch of observations, which clearly illustrates this trend.

## INTERSTELLAR EXTINCTION AND DISTANCE ESTIMATES

In this paper the determination of the interstellar extinction was based on a comparison of the theoretical relative intensities of Balmer and Paschen hydrogen lines with the observed ones. The extinction coefficient  $c(\text{H}\beta)$  was determined using about 12–15 lines for each set of spectra or, more specifically, with the application of optical Balmer lines for all spectra and additionally ultraviolet lines of this series (for the CMO spectra) or Paschen lines (for the CAS spectra). The theoretical intensities of the Balmer and Paschen lines with respect to  $\text{H}\beta$  were taken from Hummer and Storey (1987) for the following parameters:  $T_e = 10000$  K and  $N_e = 10000 \text{ cm}^{-3}$ .

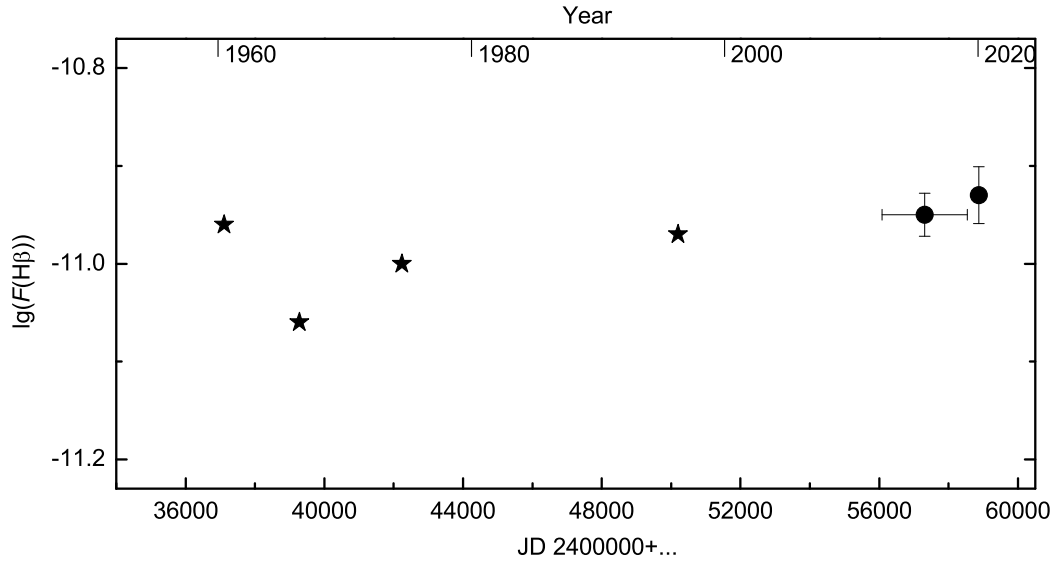


Figure 4: Time dependence of the logarithm of the  $H\beta$  flux. The measurements from Barker (1978) ( $\lg(F(H\beta))=-12$ ) are not shown. The stars and the circles indicate the data from the literature and our measurements, respectively.

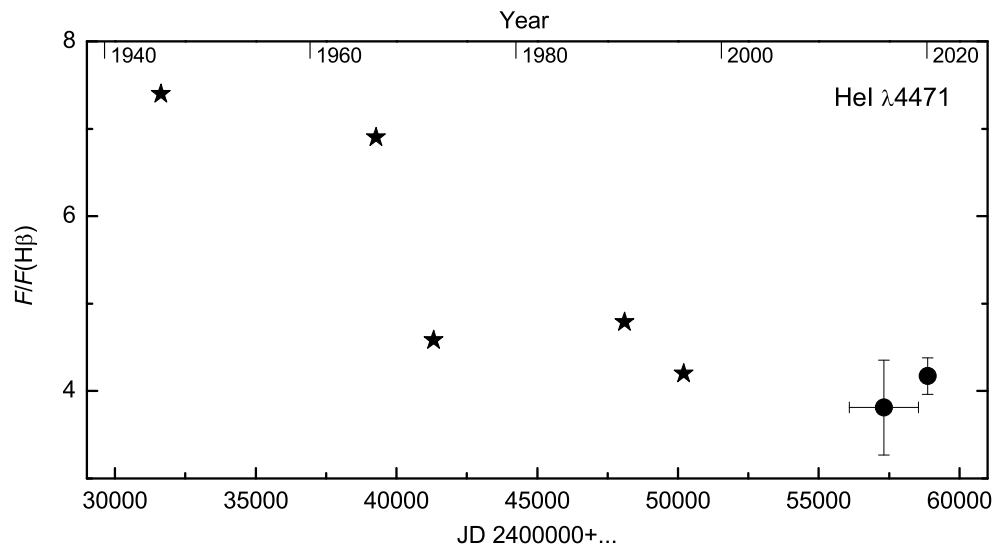


Figure 5: Change in the observed relative intensities of the He I  $\lambda 4471$  line with time. The stars and the circles indicate the data from the literature and our measurements, respectively.

The interstellar reddening curves  $f(\lambda)$  were used in the approximation from Cardelli et al. (1989), where  $R$ , the ratio of total to selective extinction, was taken to be 3.2. The correction was made using the well-known formula

$$\lg I(\lambda) - \lg F(\lambda) = c(H\beta) \cdot f(\lambda),$$

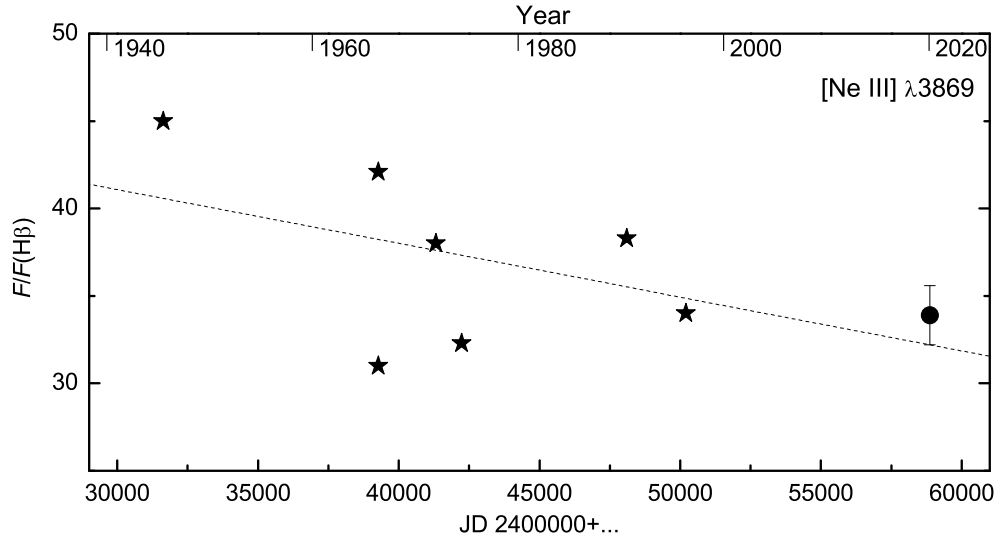


Figure 6: Change in the observed relative intensities of the [Ne III]  $\lambda 3869$  line with time. The stars and the circle indicate the data from the literature and our measurement, respectively. The dashed line represents the linear interpolation of all data.

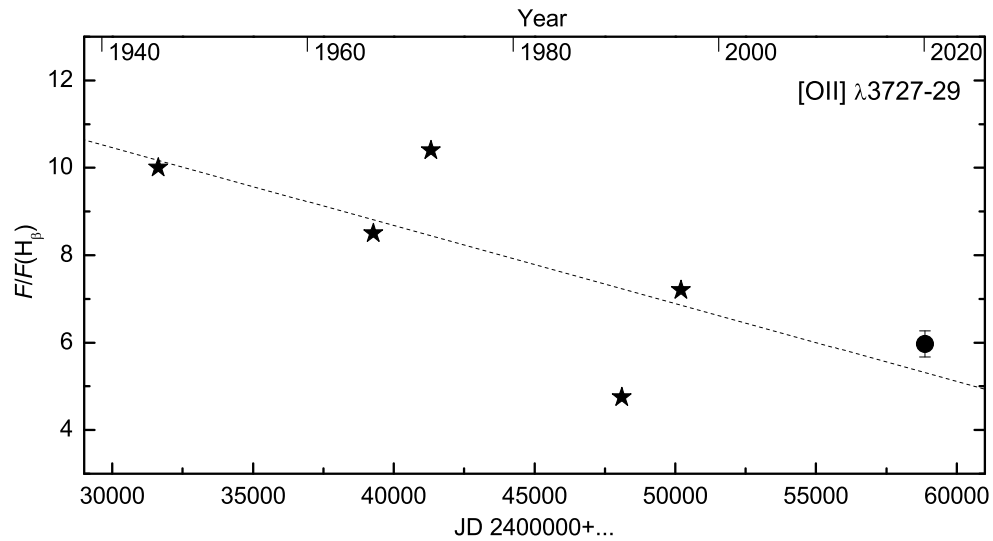


Figure 7: Change in the observed relative intensities of the [O II] doublet. The stars and the circle indicate the data from the literature and our measurement, respectively. The dashed line represents the linear interpolation of all data.

where  $F(\lambda)$  and  $I(\lambda)$  are the observed and corrected line intensities, respectively, and  $f(\lambda)$  denotes the interstellar reddening law being used.

In other papers the interstellar extinction could be taken into account by different methods: by directly determining the color excess  $E(B - V)$  by various techniques, by comparing the radio con-

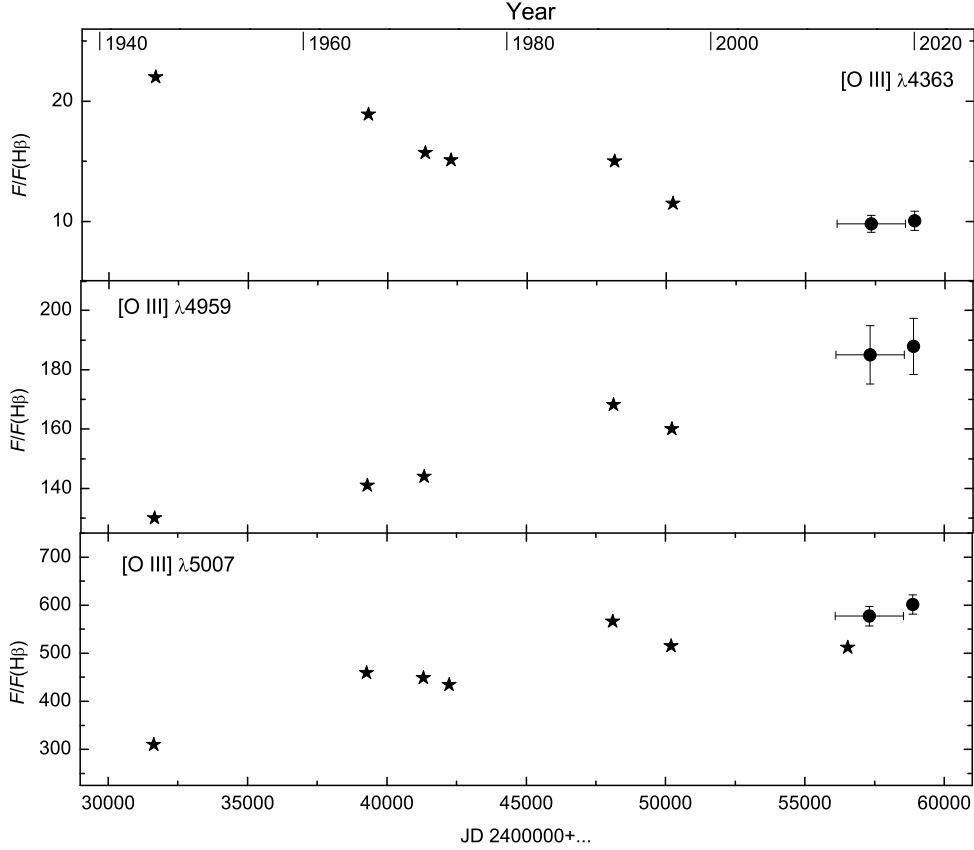


Figure 8: Change in the observed  $O^{+2}$  line fluxes with time. The stars and the circles indicate the data from the literature and our measurements, respectively.

tinuum with the emission of hydrogen lines (Preite-Martinez and Pottasch 1983), or using a larger or smaller number of Balmer and Paschen lines. For example, Kwitter et al. (2003) made a correction for reddening using only the ratio of  $H\alpha$  to  $H\beta$ . For comparison, here we provide the extinction coefficients  $c(H\beta)$  for Hb 12 derived by other authors:  $c(H\beta)=1.13$  (Barker 1978), 1.25 (Rudy et al. 1993), 1.35 (Hyung and Aller 1996), and 1.05 (Kwitter et al. 2003).

Table 4 gives the mean extinction coefficients  $c(H\beta)$ , along with the logarithm of the absolute  $H\beta$  flux, for each date of observations. The mean  $c(H\beta)$  from all our 2011-2020 data is  $1.15 \pm 0.07$ .

Table 4: The extinction coefficients and absolute fluxes in the  $H\beta$  line (in  $\text{erg s}^{-1} \text{cm}^{-2}$ ) calculated from the results of each observation

JD	$c(H\beta)$	$\lg(F(H\beta))$
2455800	1.17	-10.90
2457248	1.22	-10.92
2457667	1.16	-10.94
2457986	1.23	-10.95
2458399	1.18	-10.92
2458690	1.17	-10.97
2450702	1.01	-10.98
2458758	1.11	-10.95
2458795	1.13	-10.91
2458869	1.08	-10.94

Under conditions of a high gas density in the nebula (according to the estimates by Hyung and Aller (1996), its value in the central regions can reach  $2 \times 10^6 \text{ cm}^{-3}$ ), apart from the calculation of the extinction coefficient proper, it is necessary to study the question of possible self-absorption in hydrogen lines, because this phenomenon can distort severely the result of the correction for interstellar extinction. We followed the procedure described in Burlak and Esipov (2009) as applied to the PN IC 4997. In Fig. 9 the logarithm of the ratio  $F(\text{H}\gamma)/F(\text{H}\beta)$  is plotted against the logarithm of the ratio  $F(\text{H}\alpha)/F(\text{H}\beta)$ . The values obtained for each set of observations are plotted on the graph. It can be seen that the data points are grouped near the line corresponding to zero self-absorption, while their scatter does not exceed the measurement error.

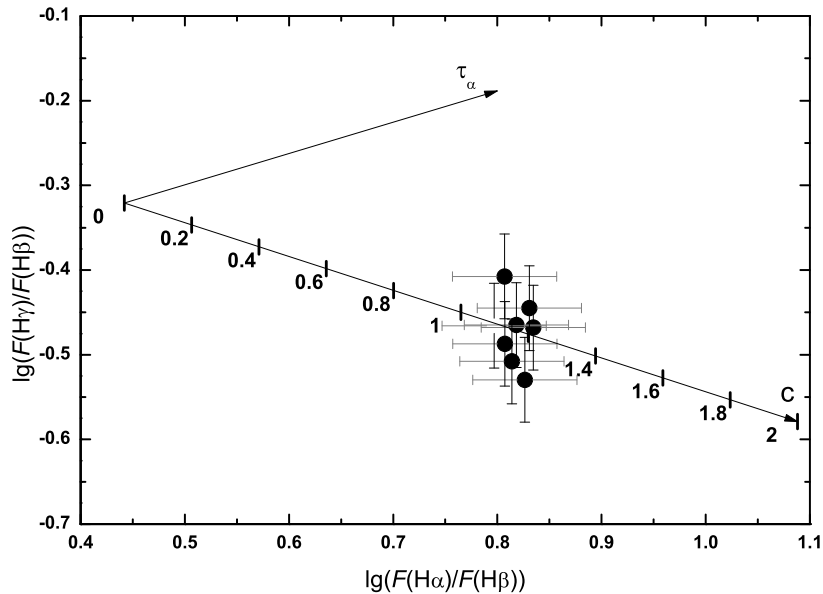


Figure 9: Logarithm of the ratio  $F(\text{H}\gamma)/F(\text{H}\beta)$  versus logarithm of the ratio  $F(\text{H}\alpha)/F(\text{H}\beta)$ . The upper arrow specifies the direction of displacement of the data points as the optical depth in the  $\text{H}\alpha$  line increases (Capriotti 1964); the lower arrow corresponds to the interstellar reddening law from Seaton (1979). The filled circles represent our results.

The distance estimation for the object is worth discussing separately.

Determining the distances to PNe is known to be an open problem. At present, no universal distance scale has been developed so far for these objects. The various statistical and semiempirical methods of determining the distances to PNe agree poorly between themselves, and for some objects these estimates can differ by several times.

Most of the Galactic PNe are extended objects, making it difficult to measure the parallax and to calculate the distance by the classical geometrical method. Nevertheless, PN researchers pin great hopes on the Gaia mission (Brown et al. 2018). The first results have already been obtained. For example, González-Santamaría et al. (2019) derived reliable distances for 211 objects from a total sample of 1571 PNe with Gaia DR2 parallaxes, while Chornay and Walton (2021) presented an updated catalogue of distances for PNe based on Gaia EDR3 data (Brown et al. 2020). For the PN Hb 12 the parallax has not yet been measured.

Yet another promising method of distance determination is based on the knowledge of the interstellar extinction toward an object. The availability of new photometric surveys, such as IPHAS (INT/WFC photometric  $\text{H}\alpha$  survey) (Drew et al. 2005), makes it possible to use the so-called extinction method to determine the distances to a large number of objects. Giammanco et al. (2011) applied this method to a sample of 137 PNe. These authors carefully studied the characteristics of

the method and the main sources of errors. The data available in the literature supplemented with new observations allowed the distances for 70 PNe to be determined. For Hb 12 a fairly uncertain estimate of  $D < 1000$  pc was obtained in this paper.

We decided to estimate the distance to Hb 12, knowing the extinction coefficient for the nebula and using the interstellar extinction maps constructed from the data of several extensive surveys (Green et al. 2019). These maps allow the distance to the object, depending on the color excess  $E(g-r)$  in the photometric SDSS system, to be determined. We converted the color excess  $E(g-r)$  to the total extinction in the  $V$  band as  $A_V = (E(g-r) - 0.03)/0.269$  (Green et al. 2019) and then to the extinction coefficient using the formula  $c(\text{H}\beta) = 1.46A_V/R$ , where  $R = 3.2$ .

In Fig. 10  $c(\text{H}\beta)$  is plotted against the distance toward Hb 12; the mean  $c(\text{H}\beta) = 1.15$  from our data and the  $c(\text{H}\beta)$  range from 1.05 (Kwitter et al. 2003) to 1.35 (Hyung and Aller 1996) from the literature are shown. Let us compare the distance  $D \approx 2400$  pc derived by us with the data of other authors. The distance to Hb 12 has been determined repeatedly. Table 5 presents some estimates with an indication of their source.

Table 5: Estimates of the distance to Hb 12 from the literature

$D$ , pc	Source
6700	Johnson et al. (1979)
3030	Kingsburg and Barlow (1992)
2236	Cahn et al. (1992)
8110	Zhang (1993)
2880	Phillips (2002)
10460	Phillips (2004)
$2260 \pm 680$	Frew et al. (2016)

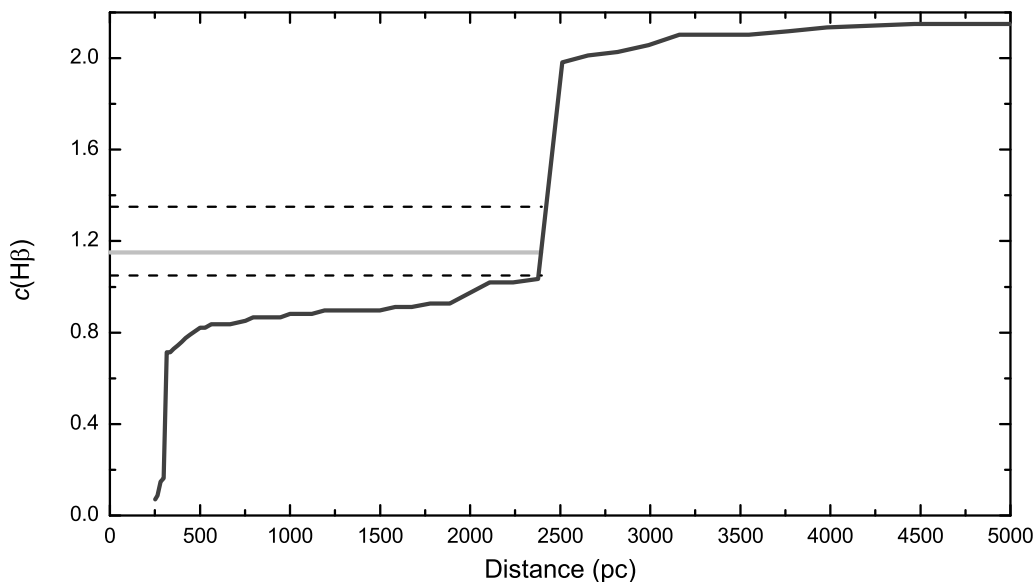


Figure 10: Extinction coefficient versus distance toward Hb 12 from the data of Green et al. (2019) (black line). The gray line corresponds to the mean extinction coefficient  $c(\text{H}\beta) = 1.15$  from our data. The dashed lines bound the range of  $c(\text{H}\beta)$  from the literature.

Our  $D$  estimate is closest to the estimates by Cahn et al. (1992) and Frew et al. (2016). It can be seen from Fig. 10 that toward Hb 12 there is a sharp increase in extinction at a distance  $> 2500$  pc

attributable to the presence of an interstellar cloud of gas and dust. Therefore, the distance to the PN Hb 12 cannot exceed 2500 pc, and its values given in Kingsburg and Barlow (1992) and, especially, Johnson et al. (1979), Zhang (1993), and Phillips (2004) should be deemed overestimated.

## DISCUSSION

Thus, we have undoubted changes in the spectrum of Hb 12 over the entire history of its spectroscopic observations. Let us now try to interpret them based on the data obtained.

Initially, it was expected that the changes in the emission-line spectrum of the nebula could be caused by the evolution of the central star. In a number of papers the nebular  $O^{+2}$  lines act as the main indicator of a change in the central star temperature. For example, Hajduk et al. (2015) studied the evolutionary changes in the relative intensity of the [O III]  $\lambda 5007$  line in the spectra of 20 PNe. For some objects these authors detected an increase in  $F(\lambda 5007)/F(H\beta)$  with time and associated it with a rise in the temperature of the ionizing source.

For Hb 12 we detected an increase in the ratio  $F(\lambda 5007)/F(H\beta)$  by a factor of  $\sim 1.9$  in 75 years.

For optically thick low-excitation PNe Kaler (1978) proposed empirical relations between the relative line intensities  $I(\lambda 5007)[O\ III]/I(H\beta)$  and  $I(\lambda 3869)[Ne\ III]/I(H\beta)$  and the temperature of the central star. We compared the temperatures derived from the proposed formulas by taking the data from this paper and the archival data from Aller (1951) as a basis. The picture turns out to be contradictory: for the [O III] line the temperature determined by this method shows a rise in 75 years from  $T_* \approx 35\ 000$  K to  $T_* \approx 44\ 000$  K, while the values of  $I(\lambda 3869)[Ne\ III]/I(H\beta)$  lead to higher estimates of the temperature and correspond to its decrease from  $T_* \approx 56\ 000$  K in 1945 to  $T_* \approx 49\ 500$  K in 2020.

In view of this contradiction, we additionally determined the temperature of the central star by the energy balance method (Preite-Martinez and Pottasch 1983; Pottasch 1987). This method is based on the idea of energy balance between the stellar radiation and the surrounding gaseous nebula and requires calculating the intensities of all the collisionally excited emission lines in the nebular spectrum. Based on our data, we found the temperature to be  $\sim 41\ 000$  K, consistent with the estimate of  $42\ 000$  K from Preite-Martinez and Pottasch (1983) obtained almost 40 years ago. Thus, the rise in the temperature of the central star in the time of spectroscopic studies of Hb 12 is still open to question.

The [O III]  $\lambda 4363$ /[O II]  $\lambda 3727$  intensity ratio, which characterizes the degree of ionization averaged over the nebula, lends support to the constancy of the temperature of the ionizing source. For Hb 12 its value probably has remained without any change over the last 75 years, while the scatter of data is due to the observational errors and the inhomogeneity of the observational data of different authors (Fig. 11).

A change in gaseous-envelope parameters seems a more obvious cause of the spectroscopic variability. Consider the most characteristic line intensity ratios that reflect the physical conditions in the nebula.

For the high-excitation zone of Hb 12 Hyung and Aller (1996) found the parameters to be  $N_e = 5 \times 10^5\ \text{cm}^{-3}$  and  $T_e = 13\ 600$  K. As was shown by Ahern (1975), in the case of a high electron density ( $N_e > 10^5\ \text{cm}^{-3}$ ), the intensity ratio of the nebular [Ne III]  $\lambda 3869$  and [O III]  $\lambda 5007$  lines depends weakly on  $T_e$  in the range  $10\ 000$ - $20\ 000$  K and, therefore, can serve as an  $N_e$  indicator.

Figure 12 shows the change in the intensity ratio of these lines with time from the published data and our new observations. From the first observations in 1945 to the mid-1960s  $F(\lambda 3869)/F(\lambda 5007)$  decreased by a factor of  $\sim 1.6$ ; in succeeding years the drop in this ratio was not so steep and the data are satisfactorily described by a linear equation.

Figure 2 in Ahern (1975) presents the theoretical dependences of  $\lg(I(\lambda 3869)/I(\lambda 5007))$  on  $\lg N_e$  for the mean ion abundance  $N(\text{NIII})/N(\text{OIII})=0.22$  for the PN.

We constructed such a diagram (Fig. 13) at some fixed temperatures (marked by the numbers in units of 1000 K) using the emissivities from the Nebulio database mentioned in Giannini et al. (2015). To construct the theoretical curves, we took the ion abundance ratio  $N(\text{NIII})/N(\text{OIII})=0.184$  based on the data for Hb 12 from Hyung and Aller (1996).

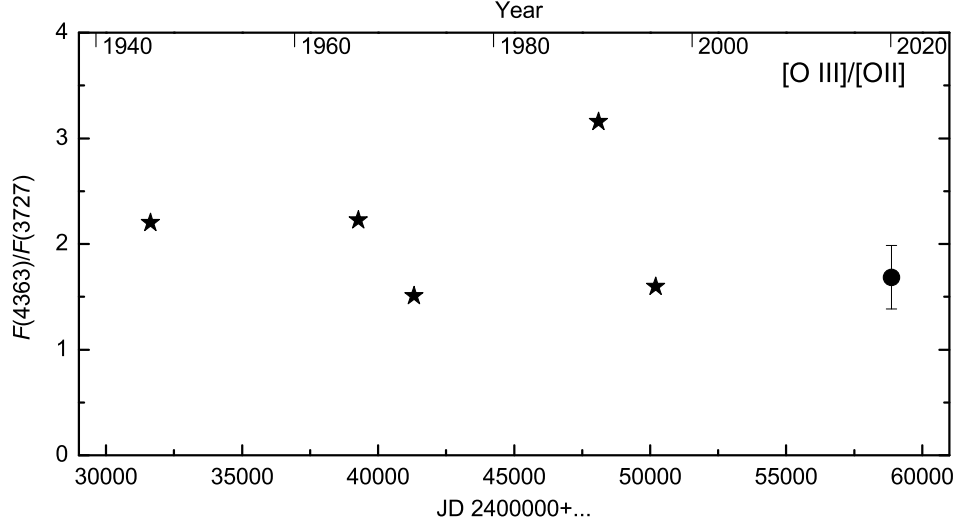


Figure 11: Intensity ratio of the [O III]  $\lambda 4363$  and [O II] ( $\lambda 3727 + \lambda 3729$ ) lines. The stars and the circle indicate the data from the literature and our measurement, respectively.

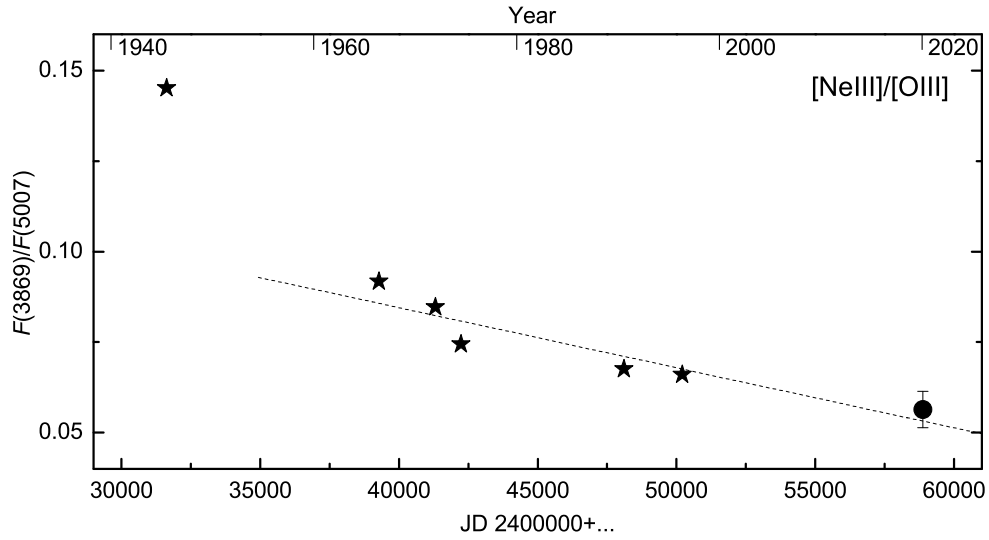


Figure 12: Intensity ratio of the [Ne III]  $\lambda 3869$  and [O III]  $\lambda 5007$  lines. The stars and the circle indicate the data from the literature and our measurement, respectively. The dashed line is the linear interpolation of the data without including the measurements of Aller (1951).

In Fig. 13 we plotted the extinction-corrected 1945, 1971, 1990, and 2020 data referring to Hb 12 and estimated  $N_e$  for different epochs. For example, if we take the range  $T_e = 10\,000 - 15\,000$  K for Hb 12, then for the first epoch  $\lg N_e \simeq 6.3 - 6.4$ , while for 2020  $\lg N_e \simeq 5.5 - 5.7$ , suggesting a drop in the electron density by a factor of  $\sim 5$  in 75 years. Such a significant change in  $N_e$  is difficult to explain by the gaseous-envelope expansion alone. At an expansion velocity of the nebula  $V_{\text{exp}} \sim 16$  km/s (Miranda and Solf 1989) its size increased by 25 % in 75 years, which will lead to a decrease in

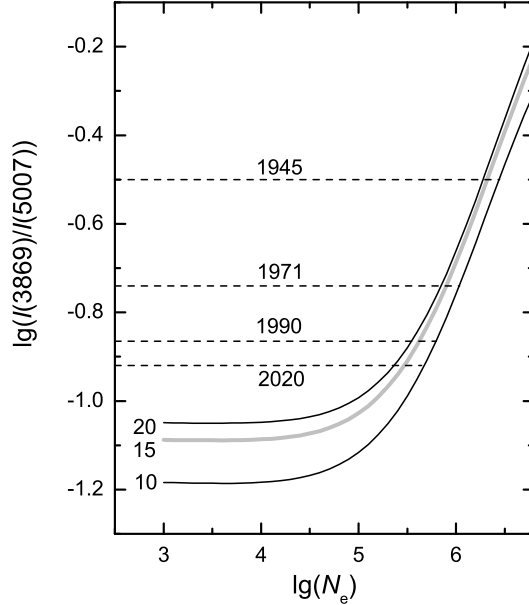


Figure 13: Logarithm of the ratio  $I(\lambda 3869)/I(\lambda 5007)$  versus electron density. The 1945, 1971, 1990, and 2020 data are those from Aller (1951), Barker (1976), Hyung and Aller (1996), and this paper, respectively.

the electron density by no more than 60 %. However, it should be noted that the central part of the nebula has a complex structure and also includes high-velocity bipolar outflows (Clark et al. 2014).

Consider the diagnostic ratio of the nebular and auroral  $O^{+2}$  lines.

Figure 14 illustrates the change in the ratio of the observed [O III] line fluxes  $F(\lambda 4959 + \lambda 5007)/F(\lambda 4363)$  with time. The graph shows a systematic increase in its value: in 75 years  $F(\lambda 4959 + \lambda 5007)/F(\lambda 4363)$  rose by a factor of  $\sim 4$ .

Table 6:  $R = I(\lambda 4959 + \lambda 5007)/I(\lambda 4363)$

Year	$R$	Source
1945	13.3	Aller (1951)
1966-1967	20.8	Kaler et al. (1976)
1971	24.9	Barker (1978)
1990	32.0	Hyung and Aller (1996)
1996	38.7	Kwitter et al. (2003)
2011-2019	51.1	This paper
2019-2020	52.1	This paper

We corrected the observed  $O^{+2}$  line fluxes for extinction with  $c(H\beta) = 1.15$ ;  $R = I(\lambda 4959 + \lambda 5007)/I(\lambda 4363)$  from the published data and our own observations are given in Table 6. The undoubted increase in  $R$  suggests a change in the parameters of the [O III] line formation region.

Suppose that the electron density did not change in the entire time of spectroscopic observations. We will take  $N_e = 5 \times 10^5 \text{ cm}^{-3}$  for it from Hyung and Aller (1996). Let us estimate  $T_e$  for different epochs using the 5Level code (De Robertis et al. 1987). We found the electron density to have decreased from 22 000 K in 1945 to 10 650 K in 2020.  $T_e \approx 13$  000 K was obtained for the epoch of observations by Hyung and Aller (1996) in 1990. Whereas this results acceptable values of the electron temperature for the last decades (1990-2020),  $T_e$  appears extremely high for the epoch of first observations, and the electron density needs to be increased to decrease  $T_e$ .

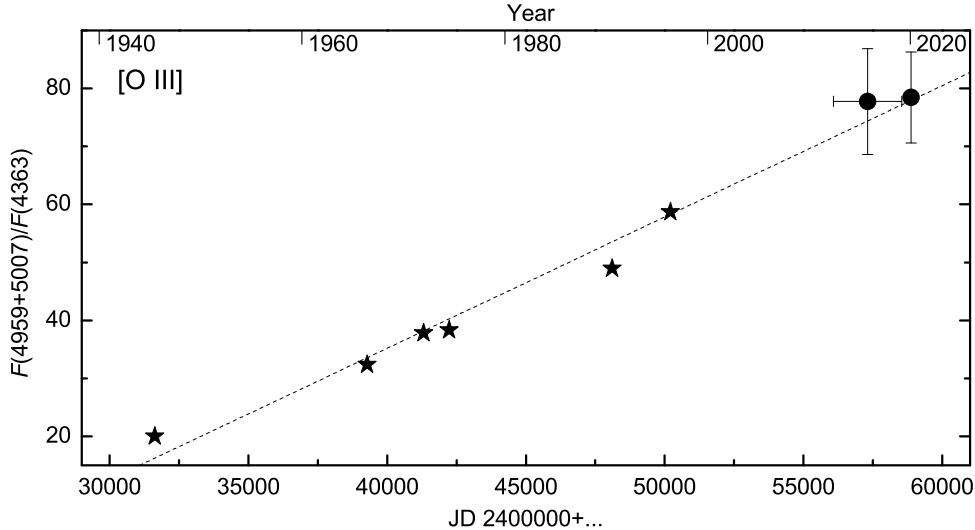


Figure 14: Time dependence of the ratio of the observed [O III] line fluxes: the stars and the circles indicate the data from the literature and our measurements, respectively. The dashed line represents the linear interpolation of all data.

As has been shown above, the temperature of the central star has remained constant over the last 40 years. Therefore, it is not yet clear what is responsible for the significant changes in the parameters of the inner PN region.

Since the parameters of the gaseous envelope of Hb 12 have been determined repeatedly using diagnostic diagrams (see, in particular, Hyung and Aller 1996; Kwitter et al. 2003) and since the diagnostic ratios  $F(\lambda 6548 + \lambda 6583)/F(\lambda 5755)$  [N II],  $F(\lambda 6717)/F(\lambda 6731)$  [S II],  $F(\lambda 7135 + \lambda 7751)/F(\lambda 5191)$  [Ar III] are determined not quite reliably, here we will not apply this method. However, in our paper we have measured for the first time the Balmer jump for the nebula, which allowed  $T_e$  to be estimated in the hydrogen emission region.

The gas electron temperature can be calculated in accordance with the formula (Liu et al. 2001)

$$T_e(BJ) = 368 \times \left( 1 + 0.259 \frac{\text{He}^+}{\text{H}^+} + 3.409 \frac{\text{He}^{2+}}{\text{H}^+} \right) \times \left( \frac{BJ}{I(\text{H}11)} \right)^{-3/2},$$

where  $\text{He}^+/\text{H}^+$  and  $\text{He}^{2+}/\text{H}^+$  express the relative abundances of neutral and ionized helium in the nebula, respectively,  $BJ$  is the Balmer jump defined as the difference of the nebular continuum intensities before and after the jump, and  $I(\text{H}11)$  denotes the intensity in the  $\lambda 3771$  hydrogen line. For Hb 12 in the 2020 CMO spectrum we measured the Balmer jump to be  $BJ = 7.06 \times 10^{-13} \text{ erg cm}^{-2} \text{ s}^{-1} \text{ \AA}^{-1}$ . The extinction-corrected line intensity  $I(\text{H}11)$  is  $7.60 \times 10^{-12} \text{ erg cm}^{-2} \text{ s}^{-1}$ ; the relative abundance of neutral helium from the data of Hyung and Aller (1996) is  $\text{He}^+/\text{H}^+ = 7.04 \times 10^{-5}$ , while the abundance of ionized helium is negligible. Our calculation based on this formula gives  $T_e(BJ) \simeq 12980 \text{ K}$ .

## CONCLUSIONS

We presented the results of our spectroscopic observations of the young compact PN Hb 12 in 2011–2020. We measured the absolute  $\text{H}\beta$  fluxes and derived the relative intensities of  $\sim 50$  nebular emission lines in the range  $\lambda 3687\text{--}9532$ .

The extinction coefficient  $c(\text{H}\beta)$  was found from Balmer and Paschen hydrogen lines. It allowed us to correct the data for interstellar reddening and to estimate the distance to the nebula by analyzing the interstellar extinction maps for the Galaxy.

Based on new and previously published data, we studied the behavior of the  $\text{H}\beta$  flux and the relative intensities of individual lines in the time of spectroscopic observations of Hb 12 from 1945 to 2020. We detected a number of probable trends, with an enhancement of the relative intensities of nebular lines and a weakening of the auroral  $\text{O}^{+2}$  line being the most significant one.

The rise in the relative intensity of the  $[\text{O III}] \lambda 5007$  line with time could be associated with an increase in the temperature of the ionizing source. However, the behavior of the relative intensity of the  $[\text{N III}] \lambda 3869$  line, which exhibited no strengthening, but showed a falling trend, does not support this hypothesis. Furthermore, the nebular core temperature estimated by the energy balance method,  $T_* \sim 41\,000$  K, virtually coincides with the value obtained almost 40 years ago (Preite-Martinez and Pottasch 1983).

Thus, we concluded that the variability of the spectrum for Hb 12 is attributable primarily to the variations in nebular parameters rather than the evolution of the central star in the post-AGB stage.

The ratio of the fluxes of the summary nebular  $\text{O}^{+2}$  lines flux to the auroral one,  $R = I(\lambda 5007 + \lambda 4959)/I(\lambda 4363)$ , showed a linear trend, while its value increased by a factor of 4 from 1945 to 2020. The electron temperature was estimated for different epochs. The value of  $T_e$  was shown to decrease with time. A decrease in the electron density in the  $[\text{O III}]$  line formation region is not ruled out either. What causes the change in the parameters of the inner PN region remains an open question.

The electron temperature of the nebula in the H I line emission region was determined from our measurements of the Balmer jump.

In addition, the CMO spectra were analyzed for the presence of absorption features that could belong to the spectrum of the cool companion of the central star. No traces of the companion were detected.

## ACKNOWLEDGMENTS

The work was performed using the equipment purchased through the funds of the Development Program of the Moscow State University. In our studies we widely used the ADS, SIMBAD, and VIZIER databases.

## REFERENCES

1. A. Acker, B. Raytchev, J. Koeppen, and B. Stenholm, *Astron. Astrophys. Suppl. Ser.* **89**, 237 (1991).
2. F. Ahern, *Astrophys. J.* **197**, 635 (1975).
3. F. Ahern, *Astrophys. J.* **223**, 901 (1978).
4. L. Aller, *Astrophys. J.* **113**, 125 (1951).
5. V. P. Arkhipova, M. A. Burlak, N. P. Ikonnikova, G. V. Komissarova, V. F. Esipov, and V. I. Shenavrin, *Astron. Lett.* **46**, 100 (2020).
6. T. Barker, *Astrophys. J.* **219**, 914 (1978).
7. T. Blöcker, *Astron. Astrophys.* **299**, 755 (1995).
8. A.G.A. Brown, A. Vallenari, T. Prusti, et al. (Gaia Collab.), *Astron. Astrophys.* **616**, 10 (2018).

9. A.G.A. Brown, A. Vallenari, T. Prusti, J.H.J. de Bruijne, C. Babusiaux, M. Biermann, O.L. Creevey, D.W. Evans, et al. (Gaia Collab.), arXiv: 2012.01533 (2020).
10. M. A. Burlak and V. F. Esipov, *Astron. Lett.* **36**, 752 (2010).
11. J.H. Cahn, J.B. Kaler, and L. Stanghellini, *Astron. Astrophys. Supp. Ser.* **94**, 399 (1992).
12. E.R. Capriotti, *Astrophys. J.* **140**, 632 (1964).
13. J.A. Cardelli, G.C. Clayton, and J.S. Mathis, *Astrophys. J.* **345**, 245 (1989).
14. N. Chornay and N.A. Walton, arXiv:2102.13654v1 (2021).
15. D.M. Clark, J.A. López, M.L. Edwards, and C. Winge, *Astron. J.* **148**, 98 (2014).
16. J.E. Drew, R. Greimel, M.J. Irwin et al., *MNRAS* **362**, 753 (2005).
17. A.V. Escudero, R.D.D. Costa, and W.J. Maciel, *Astron. Astrophys.* **414**, 211 (2004).
18. M. Faúndez-Abans and W.J. Maciel, *Astron. Astrophys.* **158**, 228 (1986).
19. D.J. Frew, Q.A. Parker, I.S. Bojčić, *MNRAS* **455**, 1459 (2016).
20. C. Giammanco, S.E. Sale, R.L.M. Corradi et al., *Astron. Astrophys.* **525**, A58 (2011).
21. T. Giannini, S. Antonucci, B. Nisini, F. Bacciotti, and L. Podio, *Astrophys. J.* **814**, 52 (2015).
22. I.N. Glushneva, V.T. Doroshenko, T.S. Fetisova, T.S. Khruzina, E.A. Kolotilov, L.V. Mossakovskaya, S.L. Ovchinnikov, and I.B. Voloshina, *VizieR Online Data Catalog III/208* (1998).
23. I. González-Santamaría, M. Manteiga, A. Manchado, A. Ulla, and C. Dafonte, *Astron. Astrophys.* **630**, A150 (2019).
24. G.M. Green, E. Schlafly, C. Zucker, J.S. Speagle, and D. Finkbeiner, *Astrophys. J.* **887**, 93 (2019).
25. M. Hajduk, P.A.M. van Hoof, K. Gesicki, A. A. Zijlstra, S. K. Górny, and M. Gładkowski, *Astron. Astrophys.* **567**, A15 (2014).
26. M. Hajduk, P.A.M. van Hoof, and A.J. Zijlstra, *Astron. Astrophys.* **573**, A65 (2015).
27. C.H. Hsia, W.H. Ip, and J.Z. Li, *Astrophys. J.* **131**, 3040 (2006).
28. E. Hubble, *PASP* **33**, 174 (1921).
29. D.G. Hummer, and P.J. Storey, *MNRAS* **224**, 801 (1987).
30. S. Hyung and L. Aller, *MNRAS* **278**, 551 (1996).
31. B.W. Jiang, Ke Zhang, A. Li, and C.M. Lisse, *Astrophys. J.* **765**, 72 (2013).
32. H.M. Johnson, B. Balick, and A.R. Thompson, *Astrophys. J.* **233**, 919 (1979).
33. J.B. Kaler, *Astrophys. J.* **220**, 887 (1978).
34. J.B. Kaler, L.H. Aller, and S.J. Czyzak, *Astrophys. J.* **203**, 636 (1976).
35. R.L. Kingsburg and M.J. Barlow, *MNRAS* **257**, 317 (1992).
36. L.N. Kondratyeva, *Astron. and Astrophys. Transactions* **24**, 291 (2005).
37. E.B. Kostyakova and V.P. Arkhipova, *Astron. Rep.* **53**, 1155 (2009).

38. K.B. Kwitter, R.B.C. Henry, and J.B. Milingo, *Publ. Astron. Soc. Pacific* **115**, 80 (2003).
39. S. Kwok and C.H. Hsia, *Astrophys. J.* **660**, 341 (2007).
40. X.-W. Liu, M.J. Barlow, M. Cohen, I.J. Danziger, S.-G. Luo, J.P. Baluteau, P. Cox, R.J. Emery, T. Lim, and D. Pequignot, *MNRAS* **323**, 343 (2001).
41. K.L. Luhman and G.H. Rieke, *Astrophys. J.* **461**, 298 (1996).
42. O. De Marco, T.C. Hillwig, and A.J. Smith, *Astron. J.* **136**, 323 (2008).
43. M.M. Miller Bertolami, *Astron. Astrophys.* **588**, A25 (2016).
44. L.F. Miranda, and J. Solf, *Astron. Astrophys.* **244**, 353 (1989).
45. C.R. O'Dell, *Astrophys. J.* **138**, 293 (1963).
46. R. Ohsawa, T. Onaka, I. Sakon, M. Matsuura, and H. Kaneda, *Astron. J.* **151**, 93 (2016).
47. M. Peimbert, in *Planetary Nebulae, Observation and Theory*, ed. Y., Terzian (Dordrecht: Reidel), *IAU Symp.*, **76**, 215 (1978).
48. M. Perinotto, *Astrophys. J. Suppl. Ser.* **76**, 687 (1991).
49. J.P. Phillips, *Astrophys. J. Suppl. Ser.* **139**, 199 (2002).
50. J.P. Phillips, *MNRAS* **353**, 589 (2004).
51. A.J. Pickles, *Astrophys. J. Suppl. Ser.* **59**, 33 (1985).
52. S. A. Potanin, A. A. Belinskii, A. V. Dodin, et al., *Astron. Lett.* **46**, 837 (2020).
53. S. R. Pottasch, *Planetary Nebulae* (Kluwer, Dordrecht, 1984).
54. A. Preite-Martinez and S.R. Pottasch, *Astron. Astrophys.* **126**, 31 (1983).
55. C. Quireza, H.J. Rocha-Pinto, and W.J. Maciel, *Astron. Astrophys.* **475**, 217 (2007).
56. M.M. De Robertis, R.J. Dufour, and R.W. Hunt, *JRASC* **81** (1987).
57. R.J. Rudy, G.S. Rossano, P. Erwin, R.C. Puetter, and W.A. Feibelman, *Astrophys. J.* **105**, 1002 (1993).
58. M.J. Seaton, *MNRAS* **187**, 73 (1979).
59. S.G. Sergeev and F. Heisberger, *A Users Manual for SPE*. Wien (1993).
60. R. Tylenda, A. Acker, and B. Stenholm, *Astron. Astrophys. Suppl. Ser.* **102**, 595 (1993).
61. E. Vassiliadis and P.R. Wood, *Astrophys. J. Suppl. Ser.* **92**, 125 (1994).
62. N.M.H. Vaytet, A.P. Rushton, M. Lloyd, J.A. López, J. Meaburn, T.J. O'Brien, D.L. Mitchell, and D. Pollacco, *MNRAS* **398**, 385 (2009).
63. C.Y. Zhang, *Astrophys. J.* **410**, 239 (1993).
64. C.Y. Zhang and S. Kwok, *Astron. Astrophys.* **237**, 479 (1991).

Translated by V. Astakhov

## Appendix: Spectroscopic Data for Hb 12

Table 7: The observed emission line intensities expressed in units of  $F(H\beta) = 100$  that were derived during the CAS observations in 2011–2019

$\lambda$ , Å	Species	F(11)	F(15)	F(16)	F(17)	F(18)	F(19)	F(19a)	F(19b)
4101	H I	12.3	18.3	14.2	-	15.8	11.3	-	-
4340	H I	33.9	33.2	34.1	37.2	34.0	31.1	39.1	34.2
4363	[O III]	10.0	9.6	9.4	10.4	9.5	9.18	12.4	8.4
4471	He I	3.68	4.08	3.41	3.40	3.37	3.91	-	-
4387	He I	-	-	-	-	-	-	0.69	-
4713	He I	0.66	0.71	0.76	-	-	1.59	0.96	0.91
4861	H I	100	100	100	100	100	100	100	100
4920	He I	-	-	-	-	-	-	2.0	0.99
4959	[O III]	183	181	189	181	186	203	183	167
5007	[O III]	574	564	586	571	584	629	570	522
5147	[Fe IV]	-	-	-	-	-	0.14	-	-
5159	[Fe II]	-	-	-	-	-	0.12	-	-
5192	[Ar III]	0.44	0.27	-	-	0.37	0.60	0.47	0.31
5270	[Fe III]	0.37	-	-	-	-	0.61	0.38	0.44
5517	[Cl III]	-	-	-	-	0.16	-	-	-
5537	[Cl III]	-	0.26	0.29	-	0.40	0.30	0.36	0.24
5577	[O I]	0.89	0.39	0.43	0.78	-	0.42	0.16	0.30
5666	N II	-	-	0.16	-	-	-	-	-
5680	N II	-	-	0.28	-	-	0.17	0.59	0.29
5755	[N II]	10.7	9.15	11.7	9.67	9.70	8.65	11.2	8.42
5876	He I	28.0	27.4	31.5	26.8	30.3	24.2	29.3	23.2
5959	O I	-	0.23	0.35	-	0.21	0.19	0.43	0.24
5979	Si II	-	0.18	0.27	-	0.20	0.24	0.39	0.17
6048	O I	-	0.31	0.40	0.26	0.26	0.23	0.38	0.24
6300	[O I]	4.63	2.43	2.91	2.93	3.29	2.47	2.91	2.45
6312	[S III]	8.02	8.56	8.40	7.88	8.55	7.69	9.54	7.48
6347	Si II	-	0.39	0.45	0.32	-	0.33	0.43	0.27
6363	[O I]	0.77	0.99	1.20	0.77	0.92	0.70	1.40	0.81
6563	H I	662	690	671	671	683	-	641	626
6584	[N II]	65.0	71.0	95.0	79.0	80.0	84.5	73.2	62.8
6678	He I	9.98	9.05	10.53	8.80	9.60	8.67	10.8	7.98
6717	[S II]	0.62	0.55	0.64	0.57	0.99	0.43	0.58	0.77
6731	[S II]	1.21	1.17	1.29	1.28	1.24	0.96	1.62	1.46
7002	O I	-	-	0.25	-	-	0.23	0.58	0.22
7065	He I	34.73	33.12	33.35	36.65	32.70	23.5	39.2	26.7
7135	[Ar III]	63.07	60.27	60.18	64.11	60.29	43.1	69.0	47.8
7236	C II	-	-	0.85	-	0.85	0.46	-	0.74
7253	O I	0.76	0.52	0.52	-	0.85	0.40	0.61	0.70
7281	He I	3.45	2.97	2.97	-	5.08	3.14	3.48	2.55
7325	[O II]	126	97.56	98.1	98	97	71.0	120.1	79.9
7376	?	-	-	-	-	-	-	0.26	-
7467	N I?	-	-	-	-	-	-	0.23	-
7751	[Ar III]	21.06	15.63	15.63	19.51	17.6	11.3	17.4	-
8323	H I	-	0.06	0.11	0.12	0.20	0.15	-	-
8334	H I	-	0.23	0.20	0.24	0.28	0.24	-	-
8346	H I	-	0.50	0.58	0.54	0.44	0.55	-	-
8361	He I	1.17	0.93	1.03	0.96	1.10	0.96	-	-
8375	H I	0.68	0.61	0.68	0.57	0.57	0.67	-	-
8392	H I	1.04	0.94	1.05	0.88	0.74	0.81	-	-
8413	H I	1.08	1.09	1.09	1.11	1.09	0.84	-	-
8442	H I/O I	10.4	8.45	7.63	7.77	9.63	7.05	10.2	-
8467	H I	2.19	1.77	1.42	1.56	1.71	1.44	-	-
8502	H I	2.87	2.24	2.19	1.95	2.22	2.02	2.82	-
8545	H I	3.22	2.41	2.30	2.17	2.67	2.53	3.12	-
8598	H I	3.65	3.11	2.35	2.59	3.34	2.43	4.16	-
8665	H I	5.40	4.19	5.11	3.82	4.33	3.36	3.50	-
8750	H I	6.32	4.51	4.06	4.57	5.20	3.64	5.27	-
8862	H I	8.19	5.65	5.36	6.07	-	4.51	6.02	-
9015	H I	10.9	-	7.05	7.31	-	5.24	7.89	-
9069	[S III]	119	-	-	82.7	102	-	92.9	-
9229	H I	-	-	-	11.64	-	-	-	-
9532	[S III]	-	-	-	198	-	-	-	-

Table 8: The observed emission line intensities expressed in units of  $F(\text{H}\beta) = 100$  that were derived during the observations at the 2.5-m CMO telescope on November 7, 2019, and January 20, 2020

$\lambda$ , Å	Species	F(19c)	F(20)	$\lambda$ , Å	Species	F(19c)	F(20)
3687	H I	-	0.54	5273	[Fe III]	0.31	0.23
3692	H I	-	0.60	5299	O I	-	0.10
3697	H I	-	0.67	5513	O I	-	0.07
3705	He I	0.75	1.20	5517	[Cl III]	-	0.08
3712	H I	0.74	1.05	5537	[Cl III]	-	0.30
3726	[SIII]/[OII]	6.12	5.75	5555	O I	-	0.14
3734	H I	1.16	1.41	5577	[O I]	-	0.12
3750	H I	-	1.89	5667	N II	-	0.32
3771	H I	-	2.34	5680	N II	-	0.19
3798	H I	-	3.06	5755	[N II]	10.5	12.1
3819	He I	1.07	0.84	5868	Si II	-	0.04
3835	HI/HeI	4.02	4.04	5876	He I	26.8	31.6
3869	[Ne III]	31.8	33.9	5932	N II	-	0.12
3889	H I	7.01	7.33	5942	N II	-	0.20
3967	[Ne III]	18.2	20.6	5958	O I	0.30	-
4009	[NeIII]/HI	-	0.19	5978	Si II	0.28	0.23
4026	He I	-	1.68	6048	O I	0.58	0.33
4069	[S II]	1.16	0.97	6300	[O I]	0.86	2.69
4076	[S II]	-	0.33	6312	[S III]	8.97	10.6
4101	H I	15.3	15.4	6347	Si II	0.42	0.42
4121	He I	0.32	0.28	6363	[O I]	0.86	0.91
4144	He I	0.29	0.24	6371	Si II	0.30	0.26
4340	H I	35.4	33.3	6461	N II	0.11	0.07
4363	[O III]	10.5	10.1	6481	N II	0.11	0.10
4388	He I	0.57	0.53	6548	[N II]	21.2	19.9
4414	[Fe II]	-	0.26	6563	H I	-	881
4471	He I	4.49	4.17	6584	[N II]	65.9	61.3
4631	N II	-	0.15	6678	He I	11.0	11.8
4641	N III	-	0.34	6717	[S II]	0.65	0.44
4649	O II	-	0.31	6731	[S II]	1.31	0.88
4676	O II	-	0.04	7002	O I	0.48	0.39
4686	He II	-	0.14	7065	He I	38.7	39.0
4701	[Fe III]	-	0.24	7136	[Ar III]	62.6	67.0
4713	He I	1.13	0.93	7155	[Fe II]	-	0.10
4740	[Ar IV]	0.19	0.22	7161	He I	-	0.11
4861	H I	100	100	7172	[Ar IV]	0.17	0.16
4921	He I	1.58	1.49	7232	C II	-	0.36
4932	[O III]	-	0.15	7236	[Ar IV]	1.44	0.75
4959	[O III]	186	188	7254	O I	1.10	0.98
5007	[O III]	598	601	7281	He I	2.76	3.26
5047	Si II	0.28	0.29	7307	O III?	1.05	1.13
5056	Si II	0.25	0.22	7319	[O II]	57.4	65.1
5147	[Fe IV]	0.22	0.18	7330	[O II]	46.3	52.6
5191	[ArIII]/[NI]	0.21	0.25	7377	[Ni II]	-	0.08
5197	[N I]	-	0.12	7444	N II	-	0.13
5263	[Fe II]	0.16	0.08				